PREDICTION OF STREAMLINE CURVATURE EFFECTS ON WALL-BOUNDED TURBULENT FLOWS

Nobuyuki Shima, Takafumi Kawai, Masayoshi Okamoto and Ryuta Tsuchikura
Department of Mechanical Engineering, Shizuoka University
Johoku 3-5-1, Hamamatsu, 432-8561, Japan

ABSTRACT

A low-Reynolds-number second-moment closure without wall-reflection redistribution terms is tested in wall-bounded turbulent flows with streamline curvature. The test cases are two fully-developed curved channel flows and four boundary layers on curved walls. The turbulence model captures main features of the stabilizing and destabilizing effects of streamline curvature, though some notable discrepancies between the predictions and measurements are present in boundary layers on convex walls.

INTRODUCTION

The "basic" second-moment turbulence closure (see Launder, 1989) and its low-Reynolds-number variants (e.g. Launder and Shima, 1989; Shima, 1993) have been widely used with success to calculate various turbulent flows. A weakness of these closures is that they contain wall-reflection redistribution terms which are formulated using the wall distance and wall-normal vector. Due to these elements, it is difficult to apply the models to flows with complex wall geometries.

Recently Shima (1998) proposed a low-Reynolds-number second-moment closure which adopted a quasi-linear rapid redistribution model but eliminated the conventional wall-reflection redistribution terms. In that paper, the model was tested in fully-developed channel flow, boundary layers in zero, adverse and favorable pressure gradients, and plane and round jets. The performance was generally good, encouraging further testing of the model in various turbulent flows.

Turbulent flow with streamline curvature is of considerable engineering interest. Testing of turbulence models in a variety of such flows is clearly needed before a sufficiently general model is establihed. In the present study, we test the second-moment closure in two curved channel flows and four boundary layers on curved walls.

TURBULENCE MODEL

In this section the second-moment closure proposed by Shima (1998) is summarized. The stress transport model can be written as

$$\frac{D}{Dt}\overline{u_iu_j} = P_{ij} - \frac{2}{3}\epsilon\delta_{ij} + \phi_{(1)ij} + \phi_{(2)ij} + T_{ij} + V_{ij} \quad (1)$$

$$P_{ij} = -\left(\overline{u_ju_k}\frac{\partial U_i}{\partial x_k} + \overline{u_iu_k}\frac{\partial U_j}{\partial x_k}\right) \quad (2)$$

$$\phi_{(1)ij} = -C_1\frac{\epsilon}{k}\left(\overline{u_iu_j} - \frac{2}{3}k\delta_{ij}\right) \quad (3)$$

$$\phi_{(2)ij} = -C_2\left(P_{ij} - \frac{2}{3}\delta_{ij}P\right) - C_3\left(D_{ij} - \frac{2}{3}\delta_{ij}P\right) - C_4k\left(\frac{\partial U_i}{\partial x_j} + \frac{\partial U_j}{\partial x_i}\right) \quad (4)$$

$$T_{ij} = \frac{\partial}{\partial x_k}\left(C_s\frac{k}{\epsilon}\overline{u_ku_l}\frac{\partial\overline{u_iu_j}}{\partial x_l}\right) \quad (5)$$

$$V_{ij} = \nu\frac{\partial^2}{\partial x_k\partial x_k}\overline{u_iu_j} \quad (6)$$

where U_i and u_i denote the mean and fluctuating velocity vectors, respectively, k is the turbulence energy, ϵ is its dissipation rate, ν is the kinematic viscosity, and the overbar implies the ensemble averaging. In Eq.(4), $P = P_{kk}/2$ is the production rate of k, and

$$D_{ij} = -\left(\overline{u_ju_k}\frac{\partial U_k}{\partial x_i} + \overline{u_iu_k}\frac{\partial U_k}{\partial x_j}\right) \quad (7)$$

The diffusion coefficient $C_s = 0.22$, and the four coefficients of redistribution terms are determined as

$$C_1 = 1 + 2.45A_2^{1/4}A^{3/4}[1 - \exp\{-(7A)^2\}]$$

Table 1 Test cases

Case	Investigators	Flow type	δ/R
1	Moser and Moin	Curved channel flow	= 0.0127
2	Kobayashi et al.	Curved channel flow	= 0.0417
3	Hoffmann and Bradshaw	Boundary layer on concave wall	$\simeq$ 0.01
4	Hoffmann and Bradshaw	Boundary layer on convex wall	$\simeq$ 0.01
5	Gillis and Johnston	Boundary layer on convex wall	$\simeq$ 0.1
6	Alving et al.	Boundary layer on convex wall	$\simeq$ 0.1

$$\times[1-\exp\{-(R_T/60)^2\}] \tag{8}$$

$$C_2 = 0.7A \tag{9}$$

$$C_3 = 0.3A^{1/2} \tag{10}$$

$$C_4 = 0.65A(0.23C_1 + C_2 - 1) + 1.3A_2{}^{1/4}C_3 \tag{11}$$

where A and A_2 are the invariants of the stress anisotropy tensor $a_{ij} = \overline{u_i u_j}/k - 2\delta_{ij}/3$ defined by

$$A = 1 - 9A_2/8 + 9A_3/8 \tag{12}$$

$$A_2 = a_{ij}a_{ji} \tag{13}$$

$$A_3 = a_{ij}a_{jk}a_{ki} \tag{14}$$

and $R_T = k^2/\nu\epsilon$ is the turbulence Reynolds number.

The transport model for ϵ is

$$\frac{D\epsilon}{Dt} = C_{\epsilon 1}\frac{\epsilon}{k}P - C_{\epsilon 2}\frac{\epsilon\tilde{\epsilon}}{k} + \frac{\partial}{\partial x_k}\left(C_\epsilon \frac{k}{\epsilon}\overline{u_k u_l}\frac{\partial \epsilon}{\partial x_l} + \nu\frac{\partial \epsilon}{\partial x_k}\right) \tag{15}$$

where

$$\tilde{\epsilon} = \epsilon - 2\nu\left(\frac{\partial k^{1/2}}{\partial x_l}\right)^2 \tag{16}$$

The coefficients $C_{\epsilon 2}$ and C_ϵ are assigned standard values, i.e. $C_{\epsilon 2} = 1.92$ and $C_\epsilon = 0.15$. For the coefficient $C_{\epsilon 1}$, the form

$$C_{\epsilon 1} = 1.44 + \beta_1 + \beta_2 \tag{17}$$

$$\beta_1 = 0.25A\min(\lambda/2.5 - 1,\ 0) - 1.4A\min(P/\epsilon - 1,\ 0) \tag{18}$$

$$\beta_2 = 1.0A\lambda^2\max(\lambda/2.5 - 1,\ 0) \tag{19}$$

$$\lambda = \min(\lambda^*, 4) \tag{20}$$

$$\lambda^* = \left[\frac{\partial}{\partial x_i}\left(\frac{k^{3/2}}{\epsilon}\right)\frac{\partial}{\partial x_i}\left(\frac{k^{3/2}}{\epsilon}\right)\right]^{1/2} \tag{21}$$

is adopted. For more details of the closure, see Shima (1998).

TEST CASES

Table 1 summarizes the test cases. In curved channel flows (Cases 1 and 2), δ denotes the channel half-width, and R is the radius of curvature of the channel centerline. For boundary layers (Cases 3 $\sim$ 6), δ denotes the boundary layer thickness, and R is the radius of curvature of the wall. Case 1 is a fully-developed flow in a circularly curved channel which Moser and Moin (1987) created by direct numerical simulation (DNS). In this case the curvature is mild. Case 2 is also a fully-developed curved channel flow from Kobayashi et al.'s (1989) experiment in which the curvature is stronger than in Case 1. Cases 3 $\sim$ 6 are boundary layer flows on curved walls taken from well-known experimental investigations. In Cases 3 and 4 (Hoffmann and Bradshaw) the curvature is mild, while Case 5 (Gillis and Johnston, 1980) and Case 6 (Alving et al., 1990) are strongly curved flows. Cases 5 and 6 include recovery flow on a flat wall downstream of the curved section. The experimental data of Cases 3, 4 and 6 are obtained from CTTM Data Library (1993).

In Cases 1 $\sim$ 3, due to instabilities associated with concave curvature, Taylor-Görtler vortices may exist. In the experiment of Case 2 the authors observed no longitudinal vortices, while in Cases 1 and 3 Taylor-Görtler vortices are present and the statistics vary in the spanwise direction. However, we make one-dimensional calculation for Case 1 as well as Case 2, and two-dimensional calculation for Case 3, as suggested for Case 3 at the 1980-81 Stanford Conference (Kline et al., 1981).

In case of fully-developed curved channel flow, the governing equations in cylindrical coordinates r-θ-z reduce to a set of ordinary differential equations. The equations were discretized by a second-order accurate finite-volume approach and then solved by an iterative method. The number of grid points was 140, concentrated toward the wall. Grid independence was confirmed by using 70 point grid without any perceptible effect on the results.

In case of boundry layer, the governing equations to be solved are obtained by applying the boundary layer approximation to the mean flow and turbulence model equations expressed in a coordinate system whose abscissa x is measured along the wall, the ordinate y being measured at right angles to it. The numerical solutions were obtained with an adapted version of the parabolic solver PASSABLE (Leschziner, 1982). For the solution procedure, see Launder and Shima (1989) and Shima (1993).

RESULTS

Figure 1 compares the second-moment closure (denoted by Sh model) with DNS data for fully-developed curved channel flow at $U_c\delta/\nu = 2990$ (Case 1), where U_c is the centerline velocity. In Fig.1(a), the mean velocity

in the streamwise direction U and the distance from the wall y are nondimensionalized with local friction velocities. In Figs.1(b) and 1(c), U_τ denotes the global friction velocity defined by analogy with the plane channel using the pressure gradient. The locations $(r-R)/\delta = -1$ and 1 correspond to the convex and concave walls, respectively. Reynolds numbers based on the predicted local friction velocities and δ are 153 at the convex side and 178 at the concave side, close to DNS values, 155 and 180, respectively. As is seen, the mean velocity and shear stress profiles are reproduced well by the prediction, though the difference between convex-side and concave-side velocity profiles is somewhat overpredicted. For the turbulence intensities the model properly yields asymmetric profiles, but does not reproduce the high anisotropy in the wall vicinity, as expected from the result for plane channel flow (Shima, 1998).

Figure 2 shows the performance in the curved channel flow with stronger curvature at $U_m\delta/\nu = 10000$ (Case 2), where U_m is the bulk mean velocity. Reynolds numbers based on the predicted local friction velocities are 456 at the convex side and 596 at the concave side, somewhat lower than DNS values, 487 and 606, respectively. As is seen from Fig.2(a), the present model cap-

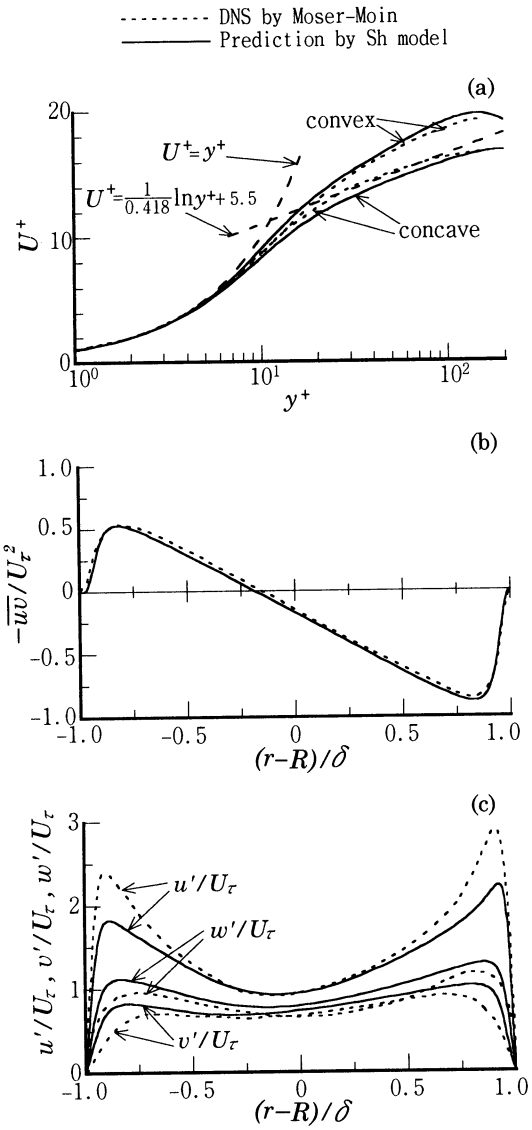

Fig.1 Curved channel flow (Case 1): (a)Mean velocity in wall coordinates (b)Shear stress (c)Turbulence intensities

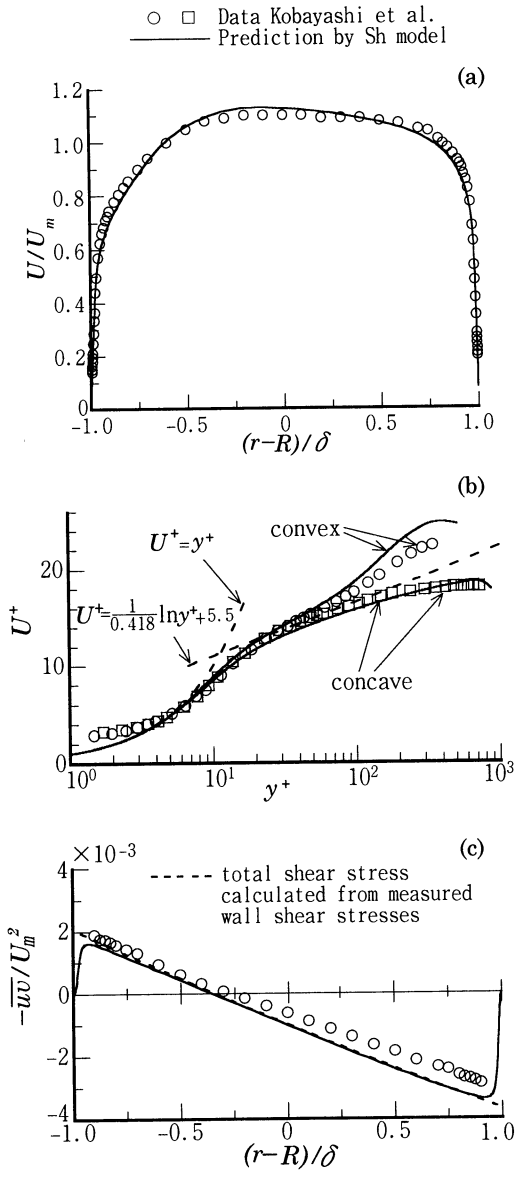

Fig.2 Curved channel flow (Case 2): (a)Mean velocity (b)Mean velocity in wall coordinates (c)Shear stress

tures the stabilizing and destabilizing effects of curvature, giving an asymmetric velocity profile close to experimental data. When plotted in wall coordinates (Fig.2(b)), the predicted convex-side profile lies above the measured profile due to the underpredicted skin friction, indicating that the model somewhat overpredicts the stabilizing effect of convex curvature. In Fig.2(c), the calculated shear stress deviates appreciably from experimental data. The figure includes a total shear stress distribution calculated from measured wall shear stresses, which is not fully consistent with the measured Reynolds shear stress. Therefore, the disagreement between the prediction and data in Fig.2(c) is not conclusive.

Turning to boundary layers, the result for the case of mild concave curvature (Case 3) is shown in Fig.3, where U_p denotes the potential flow velocity, U_{pw} is U_p at the wall, and the skin friction coefficient is defined by $C_f = 2\tau_w/\rho U_{pw}^2$(τ_w: wall shear stress, ρ: density). A prediction using another low-Reynolds-number second-moment closure (denoted by LS* model) which adopts the wall-reflection redistribution terms is also plotted for comparison. This closure is a slightly modified version (Shima, 1993) of the model proposed by Launder and Shima (1989). The response of the boundary layer to applied concave curvature is rather slow (see Hoffmann et al., 1985). As is seen from Fig.3(c), a high shear stress region grows gradually in the outer layer with increasing streamwise distance, due to the destabilizing effect of concave curvature. At the last measurement station, the region is very wide. The Sh model captures this behavior, while the LS* model does not. As shown in Fig.3(a), the skin friction also increases appreciably in the streamwise direction, and the Sh model predicts the experimental variation well. The mean velocity profiles are also reproduced faithfully by the model.

Figure 4 compares the predictions with experimental data for Case 4. In this case the effect of curvature on skin friction coefficient is less evident than in Case 3, but in the outer layer the mild convex curvature appreciably reduces the shear stress. The shear stress profiles at two stations are shown in Fig.4(c). At Station 2, just after the start of convex curvature, the outer layer quickly responds to the curvature, and the shear stress decreases considerably. This quick response contrasts with the relatively slow response to concave curvature in Case 3 (see Muck et al., 1985). The prediction with Sh model captures this quick response, but gives an excessively large reduction. As is seen from the profile at Station 3, the predicted shear stress then increases downstream, whereas the experimental data show a slow decrease. As is seen from Figs. 4(a) and 4(b), the Sh model slightly underpredicts the skin friction coefficient, and gives good predictions for mean velocity profiles.

Figure 5 shows the comparison between measurements and predictions for Case 5. The two models cap-

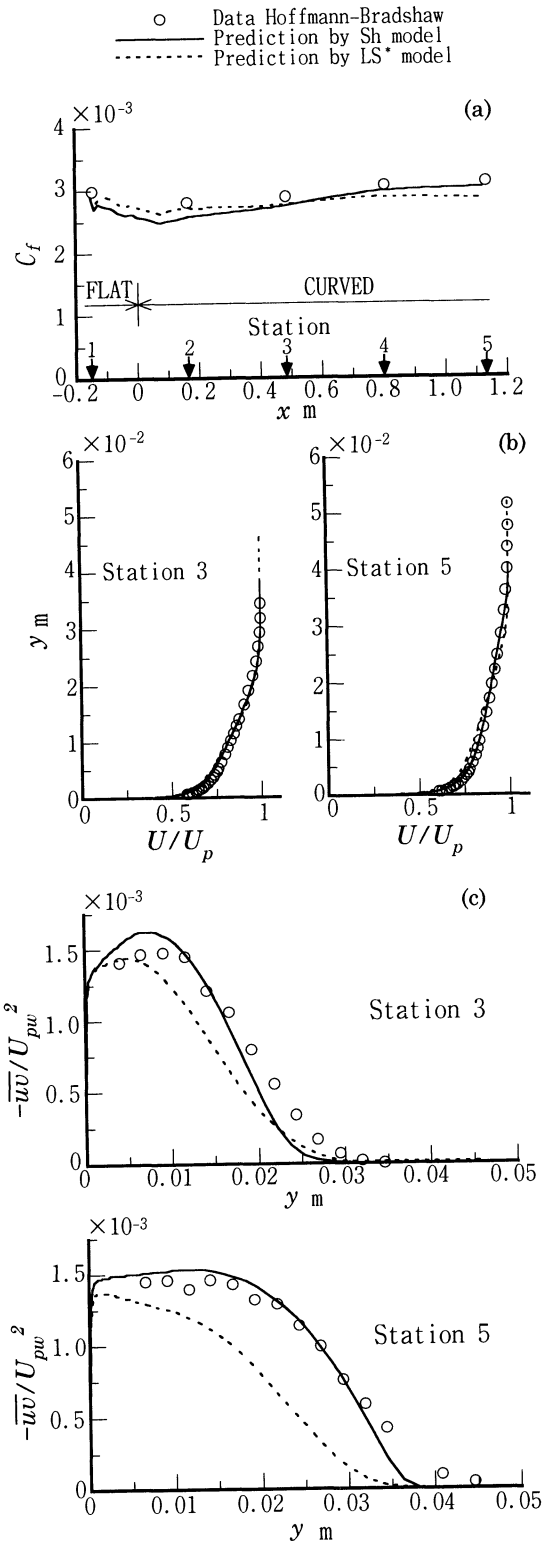

Fig.3 Boundary layer on concave wall (Case 3): (a)Skin friction coefficient (b)Mean velocity (c)Shear stress

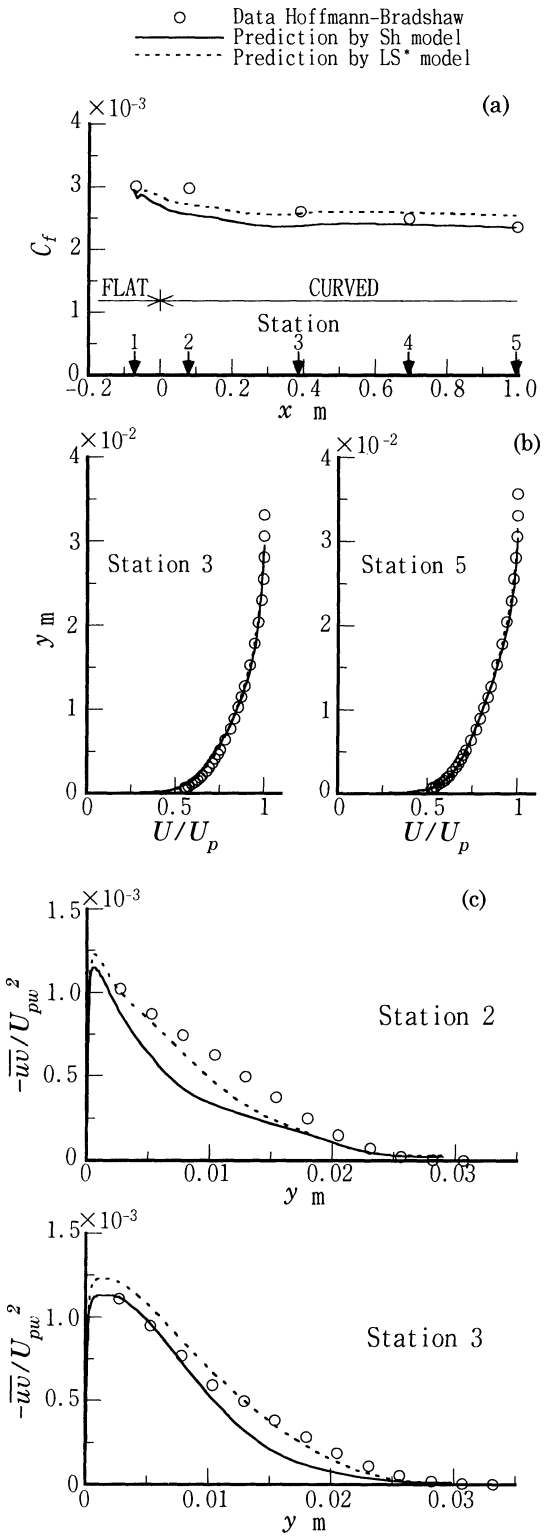

Fig.4 Boundary layer on convex wall (Case 4): (a)Skin friction coefficient (b)Mean velocity (c)Shear stress

ture the marked reduction in skin friction in the highly curved section, but the Sh model gives an excessively large reduction. In the shear stress profile at Station 5 in the curved section, the Sh model well reproduces the profile in the outer layer including a negative stress region, but underpredicts the peak value near the wall, leading to low C_f. The very slow recovery in the experiment is not captured by either of two models. In this case, overall the prediction with LS* model is closer to measurements than that with Sh model.

Finally, the streamwise variation of skin friction coefficient and the shear stress profiles for Case 6 are shown in Fig.6. This experiment concentrates on the recovery

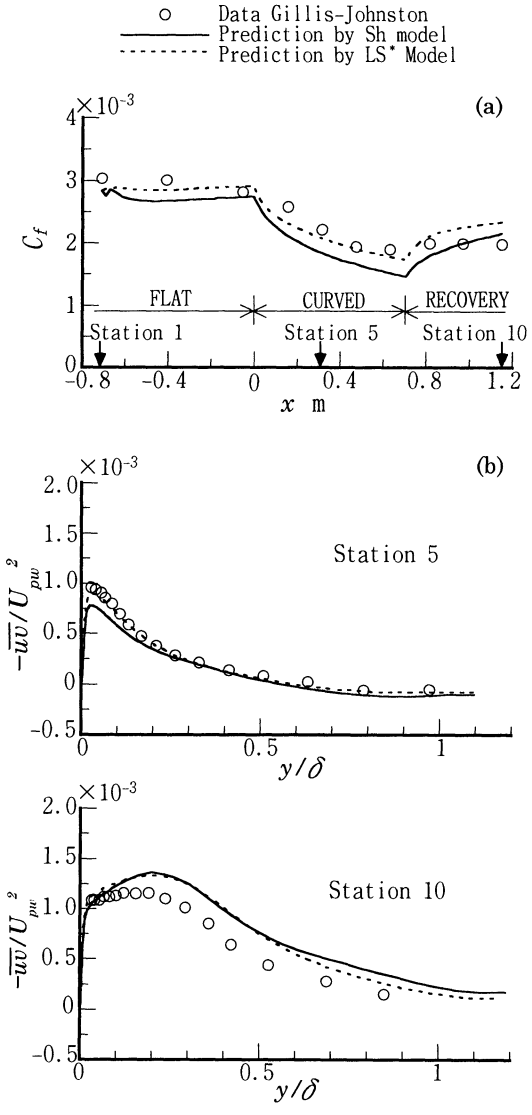

Fig.5 Boundary layer on convex wall (Case 5): (a)Skin friction coefficient (b)Shear stress

from strong convex curvature, and no measurements are available in the curved section. In the curved section steep pressure gradients exist, and the predicted skin friction varies in a complex manner under the effects of curvature and pressure gradient. In this strongly curved section, the Sh model seems to give better prediction than the LS* model, in contrast to Case 5. At Station 3, just after the removal of wall curvature, the predicted C_f agrees well with the experimental value. At this station, however, the peak value of the shear stress is overpredicted, Fig.6(b). This leads to somewhat too large skin friction in the recovery and too high level of shear stress at the last measurement station.

CONCLUDING REMARKS

A second-moment closure without wall-reflection redistribution terms has been tested in six different wall-bounded flows with streamline curvature. On the whole, the turbulence model with no curvature-specific modifications captures main features of the stabilizing and destabilizing effects of streamline curvature. As expected, the elimination of wall-reflection redistribution terms does not cause difficulties in predicting the effects of streamline curvature. In boundary layers on convex walls, some notable discrepancies between the predictions and measurements are present. We feel that it is possible to obtain better predictions by refining model functions in the redistribution term and in the dissipation-rate transport equation.

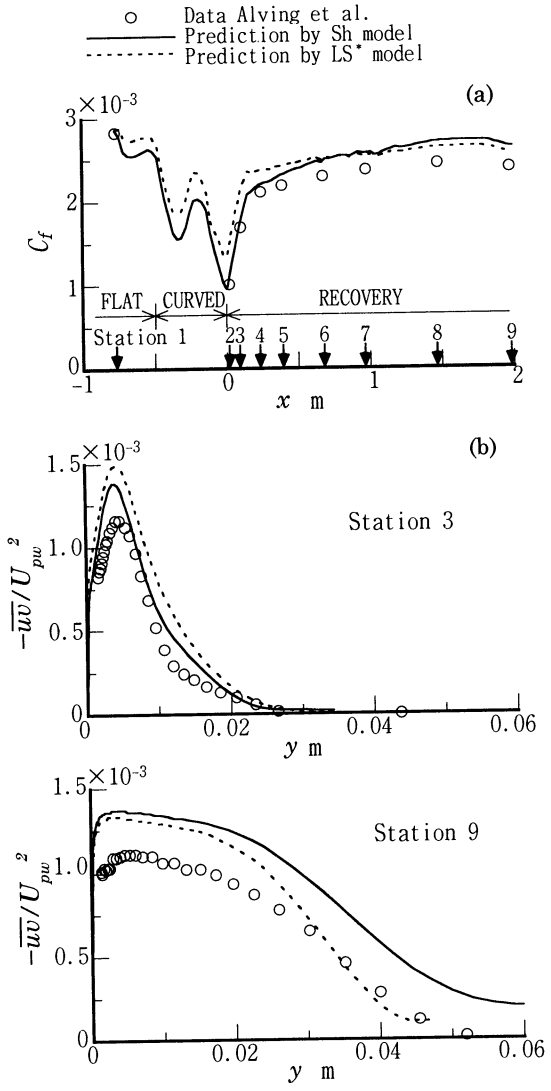

Fig.6 Boundary layer on convex wall (Case 6): (a)Skin friction coefficient (b)Shear stress

REFERENCES

Alving,A.E., Smits,A.J., and Watmuff,J.H., 1990, *J. Fluid Mech.*, Vol.211, pp.529-556.

CTTM (Collaborative Testing of Turbulence Models) Data Library, 1993, Mech. Eng. Dept., Stanford Univ.

Gillis,J.C., and Johnston,J.P., 1980, *Turbulent Shear Flows 2*, L.J.S.Bradbury et al., ed., Springer-Verlag, pp.116-128.

Hoffmann,P.H., Muck,K.C., and Bradshaw,P., 1985, *J. Fluid Mech.*, Vol.161, pp.371-403.

Kline,S.J., Cantwell,B.J., and Lilley,G.M., ed., 1981, *Proc. 1980-81 AFOSR-HTTM-Stanford Conf. on Complex Turbulent Flows.*

Kobayashi,M., Maekawa,H., Takano,T., Uchiyama, N., Kubota,M., and Kobayashi,Y., 1989, *JSME Int. J.*, Series II, Vol.32, pp.324-331.

Launder,B.E., 1989, Whither Turbulence? Turbulence at the Crossroads, J. L. Lumley, ed., Springer-Verlag, pp.439-485.

Launder,B.E., and Shima,N., 1989, *AIAA J.*, Vol.27, pp.1319-1325.

Leschziner,M.A., 1982, An Introduction and Guide to PASSABLE, Thermofluids Div., Dept. Mech. Eng., UMIST.

Moser,R.D., and Moin,P., 1987, *J. Fluid Mech.*, Vol. 175, pp.479-510.

Muck,K.C., Hoffmann,P.H., and Bradshaw,P., 1985, *J. Fluid Mech.*, Vol.161, pp.347-369.

Shima,N., 1993, ASME *J. Fluids Eng.*, Vol.115, pp.56-69.

Shima,N., 1998, *Int. J. Heat and Fluid Flow*, Vol.19, pp.549-555.